IJMSA International Journal of Microgravity Science and Application

Original Paper

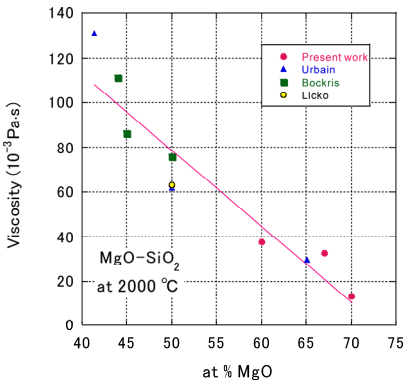
Surface Tension and Viscosity Measurements of MgO-SiO_2 Melts Using an Electrostatic Levitation Furnace Onboard the ISS

Takehiko ISHIKAWA[1*], Atsunobu MASUNO[2], Chihiro KOYAMA[1], Yuki WATANABE[1], Hirohisa ODA[1], Jumpei T. OKADA[3], Akitoshi MIZUNO[4], Yuta SHUSEKI[2], Yohei ONODERA[5], Paul-François PARADIS[6] and Shinji KOHARA[5]

[1] Japan Aerospace Exploration Agency, Tsukuba, Ibaraki Japan
[2] Kyoto University, Kyoto, Kyoto Japan
[3] Tohoku University, Sendai, Miyagi Japan
[4] National Institute of Technology, Hakodate College, Hakodate, Hokkaido Japan
[5] National Institute for Materials Science, Tsukuba, Ibaraki Japan
[6] Luqia Technologies, Quebec City, Quebec Canada

* Correspondence: Ishikawa.takehiko@jaxa.jp

Abstract: This paper reports the experimental results of surface tension and viscosity measurements of molten xMgO-(99 – x)SiO_2-1Fe_2O_3 samples (x = 30, 40, 50, 60, 67, and 70 mol%) by drop oscillation method using an electrostatic levitation furnace onboard the International Space Station (ISS). Due to their high viscosities and low electric charge on their surface, it was very difficult to excite a sufficient amount of oscillations for samples with x = 30, 40, and 50. However, surface tension and viscosity data were successfully obtained for x = 60, 67, and 70. No literature values were found for the surface tension of these compositions, while obtained viscosity values are consistent with the literature data. Limitations of drop oscillation method for surface tension and viscosity measurements are discussed.



Keywords: Electrostatic levitation, Oxide melt, Surface tension, Viscosity
Article History: Received 27 August 2026, accepted 26 October 2026, published 31 October 2026.

1. Introduction

The MgO–SiO_2 system is very important in both geoscience and glass science[1]. $MgSiO_3$ (50MgO–50SiO_2) and Mg_2SiO_4 (67MgO–33SiO_2) are Mg-end members of the main components of the Earth's mantle[2]. Mg_2SiO_4 polymorphs are considered to be the most abundant materials of Earth's upper mantle[3] and are likely a major component of an early magma ocean, present magma, and partial melts. $MgSiO_3$ and Mg_2SiO_4 exhibit quite different glass forming ability (GFA). Liquid of $MgSiO_3$ composition can be easily vitrified even with crucibles, while glassy Mg_2SiO_4 can only be obtained by levitation techniques[4]. Due to these scientific interests, structural data on the molten MgO–SiO_2 system have been measured using X-ray and neutron diffraction, NMR, and Raman spectroscopy[5–9]. Based on the obtained data, atomic structure has been studied and discussed through numerical simulations.

However, the measurements of thermophysical properties of molten MgO–SiO_2 are very limited because of their high melting temperatures. Based on the phase diagram of MgO–SiO_2 shown in **Fig. 1**[10], the lowest eutectic temperature of this system is 1560 °C, and thermophysical properties (density[11], surface tension[12,13],

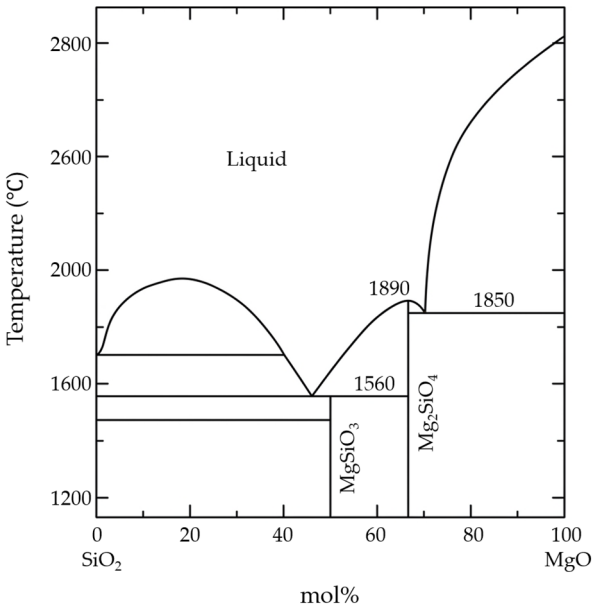


Figure 1. $MgO–SiO_2$ phase diagram[10].

viscosity[14–19]) have been measured mainly around this eutectic composition. Since the melting temperature of Mg_2SiO_4 (1890 °C) is more than 300 K higher, only a few data are available.

Viscous flow of silicate liquids is one of the primary agents of chemical and thermal evolution of the Earth, and viscosity data as a function of temperature and pressure are essential. The viscosity of Mg_2SiO_4 was measured by Urbain et al. using a rotating cup method[18]. Recently, Xie et al. measured the viscosities at high pressure by falling sphere method combined with synchrotron X-ray source[20]. No other experimental data could be found. Karki et al. calculated the viscosity of seven $MgO–SiO_2$ melts using first-principles molecular dynamics simulations[21].

The electrostatic levitation method (ESL)[22] can levitate samples using Coulomb force and allows heating them to extremely high temperature. Density[23], surface tension, and viscosity[24] can be measured from the spherical sample melted in ESL facilities. Due to insufficient surface charges, oxide samples are difficult to levitate on the ground. Therefore, an electrostatic levitation furnace onboard the ISS (ISS-ELF) has been developed and is operational for handling oxide samples in microgravity environments[25].

Samples of $MgO–SiO_2$ system in six (6) different compositions, namely $xMgO–(99 – x)SiO_2–1Fe_2O_3$ (x = 30, 40, 50, 60, 67, and 70 mol%) have been successfully levitated and melted in this facility. Results of density measurements were reported in an earlier publication[2]. This paper focuses on surface tension and viscosity measurement using the drop oscillation method. Moreover, the limitation of drop oscillation method on highly viscous samples is discussed.

2. Experimental method

High-purity powders of MgO, SiO_2, and Fe_2O_3 were stoichiometrically mixed to achieve compositions of $xMgO–(99 – x)SiO_2–1Fe_2O_3$ (x = 30, 40, 50, 60, 67, and 70 mol%). To improve the absorption of the heating laser (980 nm in wavelength), 1 mol% Fe_2O_3 was added to the samples. (Hereinafter, the samples are referred to as "xMgO".) The mixtures were pressed into pellets and sintered at 1000 °C for 12 h in air. Then, they were crushed into small pieces and melted in an aerodynamic levitation (ADL) furnace to be spherical around 2 mm in diameter. After measuring their masses, samples were put in sample holders and sent to the ISS.

Detailed descriptions on the ISS-ELF and experimental procedures for thermophysical property measurements are available elsewhere[25–27] but a concise overview is provided here for completeness. Samples are injected one at a time from the sample holder into the levitation field by a pushing rod. A sample is levitated by Coulomb force generated by three pairs of electrodes. The sample position is monitored in thre dimensions by two position-sensing systems and controlled using a high-speed feedback control scheme. Experiments are conducted in a gaseous environment at 0.2 MPa. Four semiconductor lasers heat the sample, and the sample temperature is monitored by a pyrometer. Magnified sample images are captured by a black-and-white camera from which the sample size is determined. The deformation of the sample during drop

oscillation is monitored with a power-meter onto which the sample's shadow is projected by a collimated red laser.

Once the sample is successfully molten, its temperature is maintained at a constant level by adjusting heating power of the laser. For the drop oscillation, a sinusoidal voltage is superimposed on a pair of electrodes for around 1 second, inducing oscillatory deformation of the sample (forced oscillation period). The sample deformation is detected as a fluctuation of the laser power on the power meter. If the frequency of excitation signal closely matches the mode-2 oscillation frequency of the sample, oscillation can be successfully initiated. When the excitation voltage is turned off, the sample oscillation gradually ceases due to its viscosity (natural decay period). The signal from the power meter is recorded for 5 seconds, starting from the onset of excitation, at a sampling rate of 5000 Hz. **Figure 2** depicts typical signals of natural decay obtained by the power meter, while **Fig. 3** presents the Fast Fourier Transform (FFT) results of the recorded signals. From these data, the decay time of the oscillation (τ) and resonance frequency (f_2) can be determined, allowing the calculation of surface tension (γ) and viscosity (η) using the following equations[28,29],

$$\gamma = \frac{\rho r_0^3 \left(2\pi f_2\right)^2}{8}, \tag{1}$$

$$\eta = \frac{\rho r_0^2}{5\tau}. \tag{2}$$

where ρ is the sample density and r_0 is the equilibrium sample radius. This drop oscillation experiment is performed several times by varying the excitation frequency. This procedure is repeated at different temperatures. Once the drop oscillation experiment is finished, the heating lasers are turned off to allow the sample to cool. The magnified sample images are used to calculate the density of the sample. Afterwards, the sample is returned to the sample holder, and another sample is injected to proceed with the next experiment.

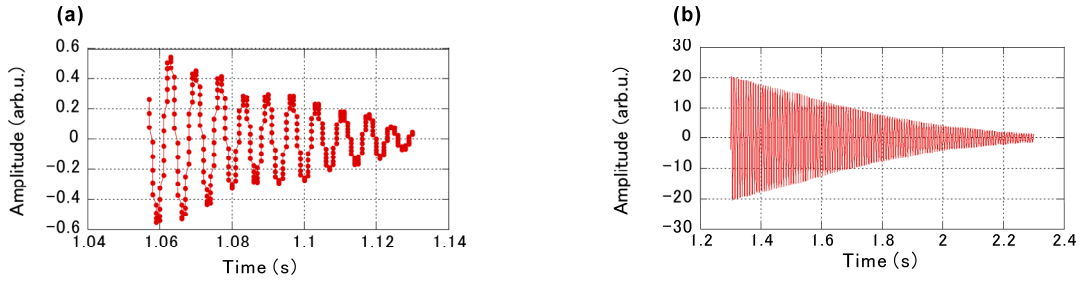


Figure 2. Typical oscillation signals during natural decay: (a) 70MgO, (b) Au.

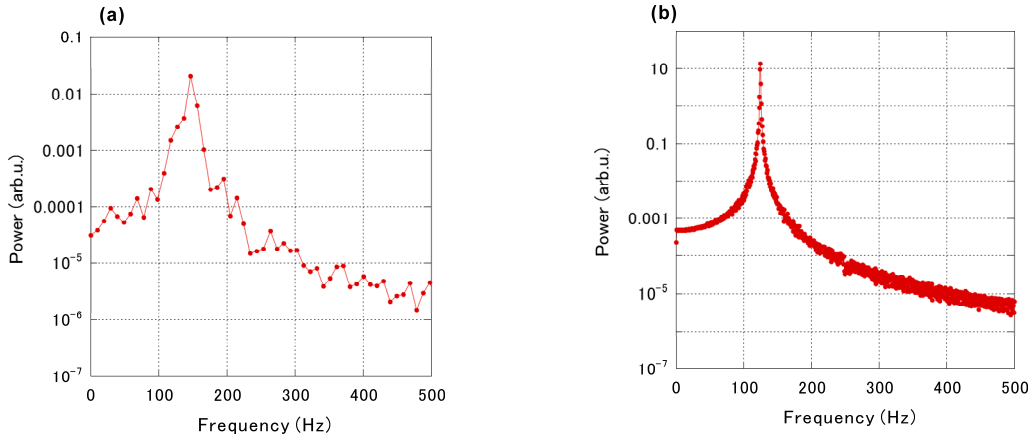


Figure 3. Results of FFT analysis on the oscillation signals in **Fig. 2**: (a) 70MgO, (b) Au.

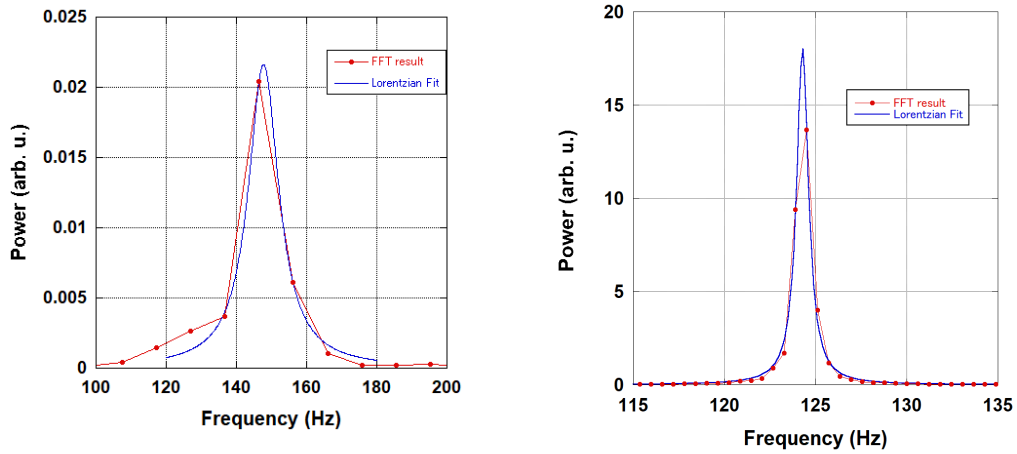


Figure 4. Lorentzian fitting on the FFT results in **Fig. 3**: (a) 70MgO, (b) Au. FWHM is 10.6 Hz (7.1%f_2) for 70MgO and 0.80 Hz (0.6%f_2) for Au, respectively.

Following the completion of the experiments, the recorded oscillation signals are downloaded from the ISS to the ground for detailed data analysis. The data are screened based on predefined quality metrics to ensure a sufficient signal-to-noise ratio and accurate measurements. First, the oscillation frequency during free decay must match (within ±1 Hz) the excitation frequency. This ensures that the forced oscillation indeed excited the mode-2 oscillation and that the accuracy of viscosity is increased. Detailed explanation is written in Appendix-A. Second, the power spectrum of the FFT result is fitted with a Lorentzian distribution as shown in **Fig. 4**. If the full width at half maximum (FWHM) of this Lorentzian function exceeds a threshold (usually set to 15% of f_2), the data are omitted. This process suppresses the uncertainty of surface tension less than around 30%. After this screening process, less than 10% of signals remain. The surface tension and viscosity are then calculated from Eqs. (1) and (2), after confirming the density by measuring the mass of the returned sample.

3. Results and discussion

The experiments on MgO-SiO_2 samples were conducted over four (4) campaigns, as summarized in **Table 1**. The first campaign, conducted in 2021, resulted in no usable oscillation data due to instability in sample positions in the liquid state, and only density data were obtained. This issue persisted during the

Table 1. Status of MgO-SiO_2 experiments in the ISS-ELF.

Campaign	Sample	Number of samples			Atmosphere
		Levitated	Density measured	Oscillation*	
1 (Mar. 2021)	50MgO	6	4	0/1	Air
	60MgO	7	2	0/4	
	67MgO	5	1	0/2	
2 (Jun. 2021)	30MgO	3	1	0	Air
	40MgO	6	2	0	
	67MgO	5	0	1/2	
	70MgO	3	3	0/2	
3 (Sep. 2022)	70MgO	3	2	1/2	Air
4 (Jul. 2024)	30MgO	3	1	0/2	Ar
	40MgO	5	2	0/2	
	50MgO	5	0	0	
	60MgO	5	2	3/5	

* Data obtained/Attempt

second campaign, although oscillation data of 67MgO were fortunately obtained. During the third campaign, improvements in the sample position control led to the successful measurement of oscillation data for 70MgO. The fourth campaign was conducted in the argon gaseous environment to improve sample stability at high temperature. Oscillation data for 60MgO were successfully obtained. Throughout these campaigns, no reliable oscillation data were observed for 30MgO, 40MgO, and 50MgO, primarily due to their high viscosity. Typical oscillation signals and FFT results are shown in Appendix-B.

The drop oscillation experiments lasted more than 30 minutes, making mass loss due to evaporation a critical issue. **Table 2** shows the sample mass values measured before and after experiments.

Evidently, the mass loss of 60MgO samples was larger than that of 67MgO and 70MgO, as the experiments were conducted over a higher temperature range. Concerns were raised regarding whether the stoichiometry of the sample was maintained. **Figure 5** illustrates the measured liquidus density of 60MgO samples. The density of 60MgO measured after the drop oscillation experiments and the density measured without drop oscillation (cooled down immediately after melting) agreed within experimental uncertainty (2.3%). Judging from those density data, compositional change can be considered negligible.

Table 2. Mass reduction during drop oscillation experiment.

Sample	Mass (mg)		Mass loss	Temperature Range	Remarks
	Before	After	(%)	(°C)	
60MgO-1	9.60	9.15	4.7	2128–2200	one sample (60MgO-3) was lost during experiment
60MgO-2	9.06	8.29	8.5	2200–2269	
67MgO	11.1	10.8	2.7	2030–2180	
70MgO	8.69	8.63	0.7	1966–2031	

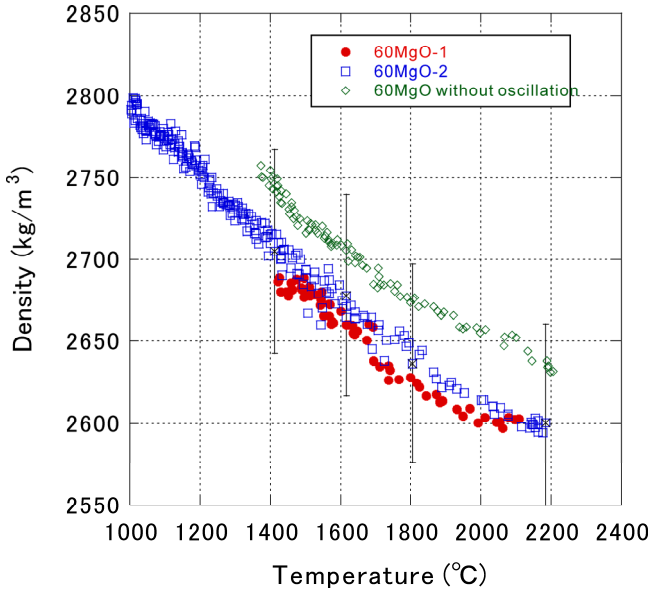


Figure 5. Density of molten 60MgO as a function of temperature. Error bars indicate 2.3% experimental uncertainties.

3.1. Surface tension

The measured surface tensions as a function of temperature, together with literature data, are shown in **Fig. 6**. Only two sets of literature data have been found. King et al. measured the magnesium-silicate samples with compositions ranging from 45.2 to 51 mol%MgO and temperature between 1550 and 1650 °C using the ring method[12]. Tokunaga et al. used the same method to measure a sample with 45.2 mol%MgO[13]. Both studies reported that surface tensions exhibited a positive temperature dependence. This temperature dependence was also observed in molten SiO_2[30,31] and is believed to reflect the changes in the liquid structure

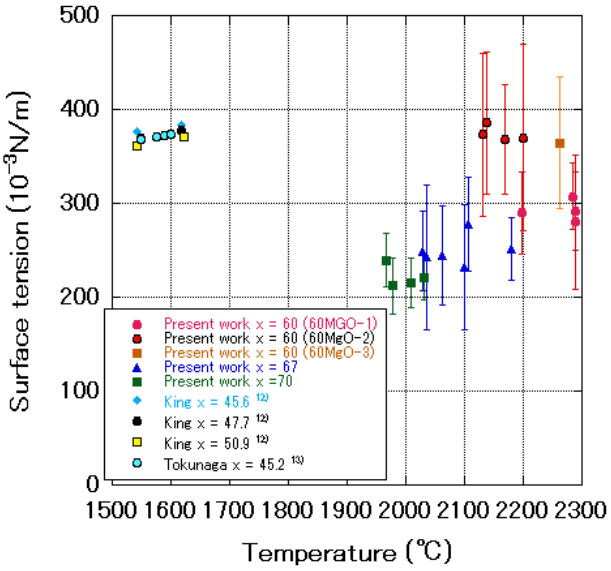


Figure 6. Measured surface tension of molten MgO–SiO_2 as a function of temperature.

of silicate[12,13,32]. Judging from the result of our literature search, surface tensions have been meaured for the first time for these compositions. While our results are valuable, it remains challenging to confirm whether the surface tensions of 60MgO, 67MgO, and 70MgO samples exhibit a positive temperature dependence. Moreover, our surface tension data show a negative compositional dependence on MgO which appears unusual given that the surface tension of MgO[33] is much higher than that of SiO_2. It is very hard to quantitatively determine the surface tensions and their temperature/compositon dependences with such huge experimental uncertainties shown in **Fig. 6**. This concern will be discussed in Sec. 3.3.

3.2. Viscosity

The measured values of viscosity along with literature data as a function of temperature are shown in **Fig. 7**. Like the data for surface tension, almost all literature data[15–17] for viscosity were measured around the eutectic composition ranging between 40 and 50 mol%MgO. The only data close to our results in both composition and temperature were taken by Urbain et al. using rotating cup method[18], as shown in **Fig. 7 (b)**. Our results show good agreement with those of Urbain. Viscosity exhibits a negative MgO composition dependence. It is well known that the viscosity of liquids exhibits Arrhenius-type temperature dependence.

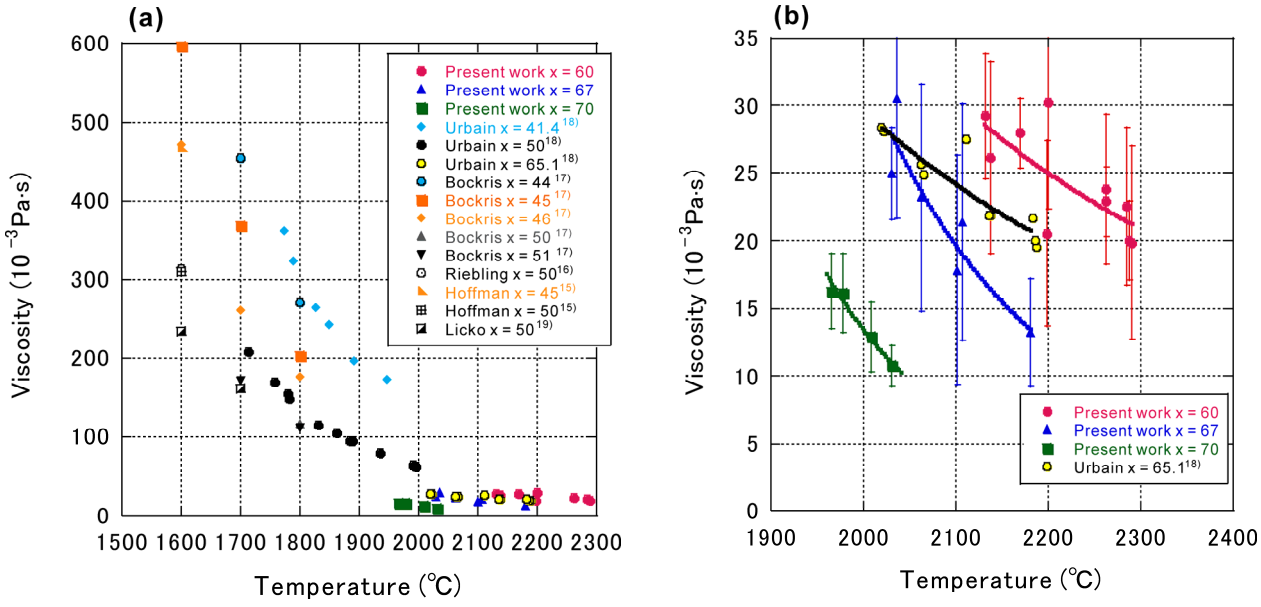


Figure 7. Measured viscosity of molten MgO-SiO_2 system vs temperature. (a) Overall; and (b) a closer view around present works.

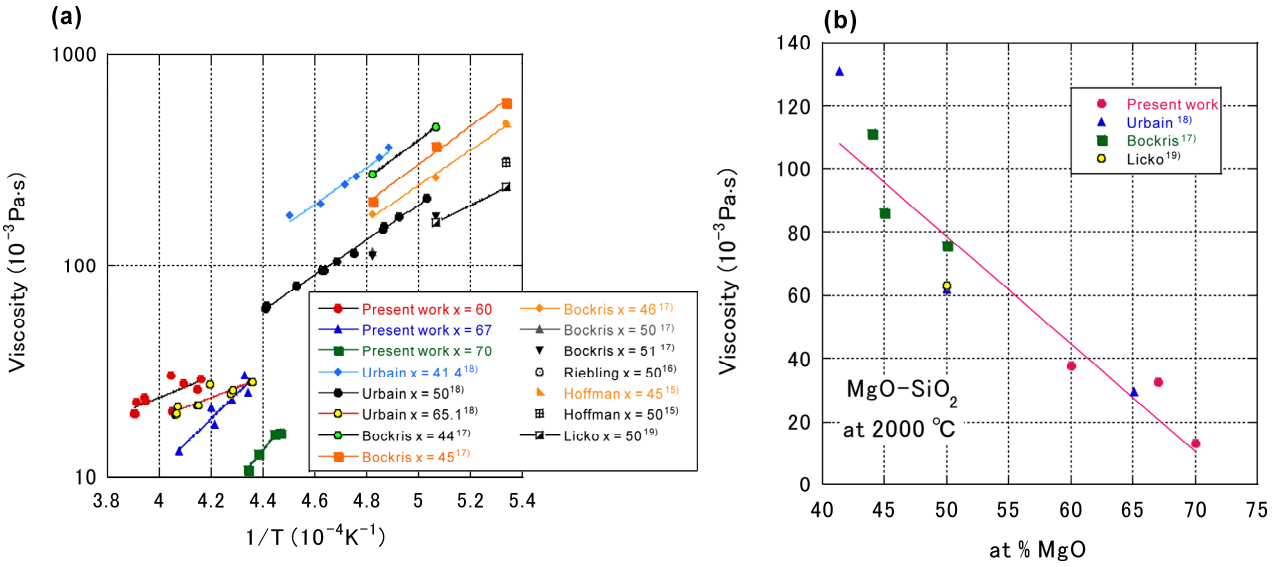


Figure 8. (a) measured viscosity of MgO–SiO_2 vs reciprocal temperature. (b) Calculated viscosity value at 2000 °C vs MgO composition.

As shown in **Fig. 8 (a)**, viscosity of MgO-SiO_2 fits Arrhenius equation well. By extrapolating and interpolating the measured data, viscosities at 2000 °C are calculated and their composition dependence is shown in **Fig. 8(b)**. Overall, viscosity of MgO–SiO_2 decreases almost linearly with increasing MgO concentration.

3.3. Experimental uncertainty

The experimental uncertainties of surface tension and viscosity can be calculated from the Eqs. (1) and (2). The relative uncertainty of surface tension ($\Delta\gamma/\gamma$) and that of viscosity ($\Delta\eta/\eta$) can be expressed by the following equations;

$$\frac{\Delta\gamma}{\gamma} = \sqrt{\left(\frac{\Delta\rho}{\rho}\right)^2 + \left(\frac{2\Delta f_2}{f_2}\right)^2 + \left(\frac{3\Delta r_0}{r_0}\right)^2} \tag{3}$$

$$\frac{\Delta\eta}{\eta} = \sqrt{\left(\frac{\Delta\rho}{\rho}\right)^2 + \left(\frac{\Delta\tau}{\tau}\right)^2 + \left(\frac{2\Delta r_0}{r_0}\right)^2} \ . \tag{4}$$

The relative uncertainty of sample radius measurement ($\Delta r_0/r_0$) is 0.8%, and thus that of density ($\Delta\rho/\rho$) is 2.4%. The uncertainty of mode 2 resonance frequency ($\Delta f_2/f_2$) can be estimated from the FWHM shown in **Fig. 4**. In the present work, ($\Delta f_2/f_2$) is set equal to FWHM, and calculated uncertainty values are plotted as error bars in **Fig. 6**. Due to their high viscosities, the durations of free decay for these samples are much shorter than those of metallic samples, with typical examples shown in **Fig. 2.** The duration of natural decay (t) for 70MgO (**Fig. 2(a)**) is 0.07 seconds, which is approximately 28 times shorter than that of Au (around 2.0 s, in **Fig. 2(b)**). Since the frequency resolution of FFT analysis is inversely proportional to t, Δf_2 for 70MgO is 28 times larger than that of Au, leading to a significantly higher uncertainty. This also affects the uncertainties of the damping constant ($\Delta\tau/\tau$) and viscosity ($\Delta\eta/\eta$).

The duration t is closely related to the relaxation time τ. From **Fig. 2**, the free decay can be observed in the ISS-ELF from the end of excitation to when the oscillation amplitude decays to 1/10 of its initial value. Therefore, t is roughly determined as follows.

$$t \approx 2.3\tau = 0.46\frac{r_0^2}{(\eta/\rho)}. \tag{5}$$

Based on Eq. (5), when the sample size is constant, t is inversely proportional to the kinematic viscosity ($\nu \equiv \eta/\rho$). Therefore, t and the uncertainty of surface tension ($\Delta\gamma/\gamma$) are directly determined by the kinematic viscosity of the sample. Also, when the desired uncertainty of the surface tension is determined, the maximum kinematic viscosity of the sample is determined. **Figure 9** depicts the result of a case study. In this study, the maximum $\Delta\gamma/\gamma$ is set to be 0.3, and Δf_2 is determined to be 1/t. The maximum kinematic viscosities are plotted as a function of mode-2 oscillation frequency of the sample (f_2), and sample radius. The maximum sample

viscosity can be slightly expanded by using bigger samples. The measurements are easier if the sample has relatively high surface tension.

The ISS-ELF has been operational for 10 years, during which numerous oxide samples[27,34–36] as well as metal[37]/alloy[38–42] samples have been processed. Drop oscillation experiments have been conducted mainly for oxide samples as summarized in **Table 3** and **Fig. 10**.

For samples containing heavy rare-earth elements, their large densities result in low kinematic viscosity, allowing relatively good oscillation signals to be obtained even when their dynamic viscosities are very high. Conversely, for oxides composed of light elements such as Al_2O_3, $CaAl_2O_4$, Al_2O_3–SiO_2, and MgO–SiO_2, measurements are extremely difficult due to their high kinematic viscosity. Judging from **Fig. 9**, the maximum

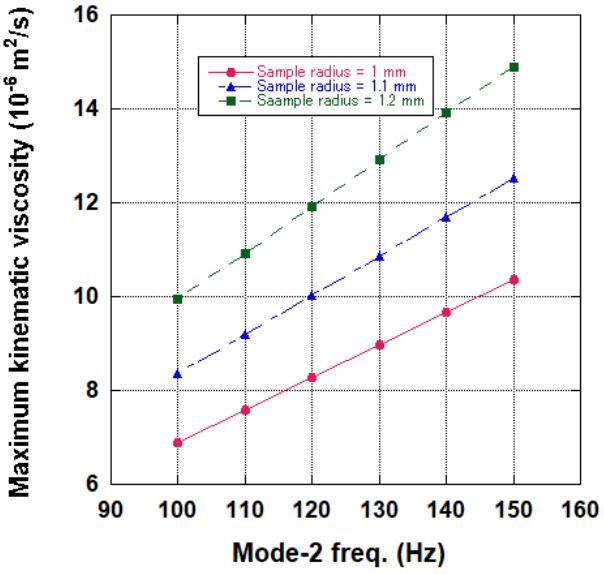


Figure 9. Maximum kinematic viscosity of the sample measurable in the ISS-ELF, with experimental uncertainty of surface tension below 0.3.

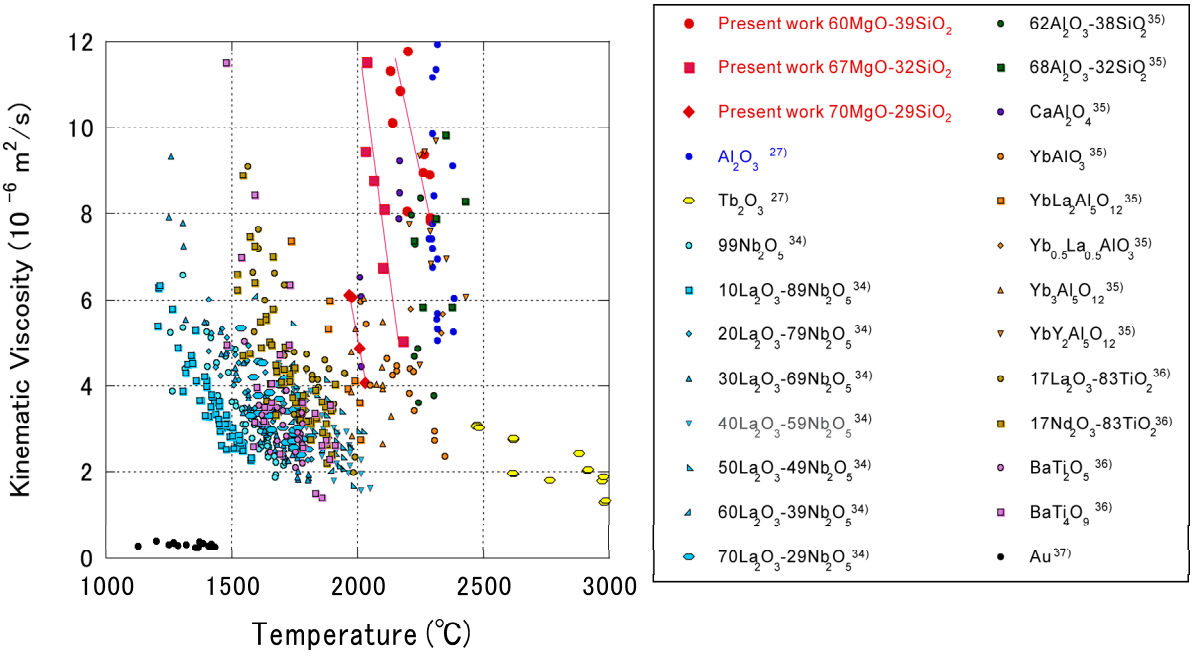


Figure 10. Kinematic viscosities of molten samples measured in the ISS-ELF.

Table 3. Density, viscosity, and kinematic viscosity of molten samples measured with the ISS-ELF.

Sample	Temperature (℃)	Density (kg/m^3)	Viscosity (mPa·s)	Kinematic Viscosity (cSt)	REF
60MgO–39SiO_2–1Fe_2O_3	2128–2269	2532–2584	19.9–30.3	7.8–11.8	Present work
67MgO–32SiO_2–1Fe_2O_3	2030–2180	2629–2648	13.3–30.5	5.0–11.5	Present work
70MgO–29SiO_2–1Fe_2O_3	1966–2031	2649–2658	10.8–16.3	4.1–6.1	Present work
Al_2O_3	2284–2384	2788–2796	14.1–33.3	5.1–11.9	27
Tb_2O_3	2472–2986	7338–7483	9.4–23.2	1.3–3.1	27
99Nb_2O_5–1Fe_2O_3	1255–1712	4186–4417	8.0–28.9	1.9–6.6	34
10La_2O_3–89Nb_2O_5–1Fe_2O_3	1207–1578	4450–4678	10.1–29.6	2.3–6.3	34
20La_2O_3–79Nb_2O_5–1Fe_2O_3	1382–1818	4638–4875	10.5–29.3	2.3–6.0	34
30La_2O_3–69Nb_2O_5–1Fe_2O_3	1251–1806	4751–5125	8.6–47.8	1.8–9.3	34
40La_2O_3–59Nb_2O_5–1Fe_2O_3	1665–2049	5026–5256	7.9–23.8	1.6–4.5	34
50La_2O_3–49Nb_2O_5–1Fe_2O_3	1711–2022	5022–5359	8.8–29.2	1.7–5.5	34
60La_2O_3–39Nb_2O_5–1Fe_2O_3	1596–1899	5309–5467	10.8–33.4	2.0–6.1	34
70La_2O_3–29Nb_2O_5–1Fe_2O_3	1490–1818	5435–5628	13.1–29.9	2.4–5.3	34
62Al_2O_3–38SiO_2	2215–2302	2759–2762	10.0–23.1	3.6–8.3	35
68Al_2O_3–32SiO_2	2226–2429	2792–2803	16.3–27.5	5.8–9.8	35
$CaAl_2O_4$	2010–2168	2755–2772	12.3–25.4	4.4–9.2	35
$YbAlO_3$	2012–2347	6007–6113	14.1–36.5	2.3–6.0	35
$YbLa_2Al_5O_{12}$	1736–2011	4611–4659	12.7–34.3	2.8–7.4	35
$Yb_{0.5}La_{0.5}AlO_3$	2211–2340	5292–5320	27.6–30.7	5.2–5.8	35
$Yb_3Al_5O_{12}$	1975–2134	5461–5489	14.5–33.1	2.7–6.0	35
$YbY_2Al_5O_{12}$	2205–2431	4480–4515	20.2–43.6	4.5–9.7	35
17La_2O_3–83TiO_2	1564–1989	4386–4540	8.7–41.3	1.9–9.1	36
17Nd_2O_3–83TiO_2	1521–1911	4494–4697	9.9–41.6	2.2–8.9	36
$BaTi_2O_5$	1414–1619	3978–4025	8.4–20.3	2.1–5.0	36
$BaTi_4O_9$	1477–1912	3812–3948	5.4–45	1.4–11.5	36
Au	1129–1434	16086–17679	4.3–6.8	0.25–0.40	37
50MgO–50SiO_2	2000	2530	62	24.5	Estimated
40MgO–60SiO_2	2000	2464	131	53.2	Estimated

measurable kinematic viscosity in the ISS-ELF is 12 cSt (10^{-6} m^2/s). This result agrees with the case study shown in **Fig. 9**. The estimated kinematic viscosities of 50MgO and 40MgO are listed in **Table 3**. Because their kinematic viscosities are far above the threshold, it is understandable that oscillation data could not be obtained for these samples with the ISS-ELF.

This limitation heavily depends on the instruments and will drastically expand if t increases. Work is currently underway to improve the oscillation system of the ISS-ELF to generate larger sample deformations.

It is important to have long observation time to accurately measure the mode-2 oscillation frequency. It is reported that 16-s observation time is required in the surface tension measurement with an electromagnetic levitator[43]. Surface tension measurement using the data of forced oscillation period, which is much longer than that of free decay, is also under consideration.

Nonetheless, the surface tension and the viscosity of MgO–SiO_2 samples with a high MgO concentration (x>60) have been measured.

4. Conclusions

Using the ISS-ELF, surface tension and viscosity values of xMgO–(99 – x)SiO_2–1Fe_2O_3 (x = 60, 67, and 70) have been obtained. In addition, over 10 years of experiments in the ISS, the limitations of drop oscillation

method, as it has been implemented, have been revealed in this study and the need for new methods is highlighted for very viscous melts.

Acknowledgments

The authors are grateful to the ISS crew members and to the ground operation staff for their support during the onboard experiments. This work was supported by JSPS Grants-in-Aid for Transformative Research Areas (A) "Hyper-Ordered Structures Science" (Grant Nos. 20H05882 and 20H05878).

Dr. Akitoshi Mizuno passed away before the publication of this manuscript. The co-authors honor his memory and invaluable contribution to this work.

Conflicts of Interest

The authors declare no conflict of interest.

References

1) B. Mysen and P. Richet: Silicate Glasses and Melts, 2nd ed. Elsevier (2019).
2) Y. Shuseki, S. Kohara, T. Kaneko, K. Sodeyama, Y. Onodera, C. Koyama, A. Masuno, S. Sasaki, S. Hatano, M. Shiga, I. Obayashi, Y. Hiraoka, J. Okada, A. Mizuno, Y. Watanabe, Y. Nakata, K. Ohara, M. Murakami, M. Tucker, M. McDonnell, H. Oda and T. Ishikawa: J. Phys. Chem. A, **128** (2024) 716, DOI: 10.1021/acs.jpca.3c05561.
3) D.B. Ghosh and B.B. Karki: Geochim. Cosmochim. Acta, **75** (2011) 4591, DOI: 10.1016/j.gca.2011.05.030.
4) S. Kohara, K. Suzuya, K. Takeuchi, C.K. Loong, M. Grimsditch, J.K.R. Weber, J.A. Tangeman and T.S. Key: Science **303** (2004) 1649, DOI: 10.1126/science.1095047.
5) C.D. Yin, M. Okuno, H. Morikawa and F. Marumo: J. Non-Cryst. Solids, **55** (1983) 131, DOI: 10.1016/0022-3093(83)90013-3.
6) Y. Waseda and J.M. Toguri: Metall. Mater. Trans. B, **8** (1977) 563, DOI: 10.1007/BF02658623.
7) S. Kohara, J. Akola, H. Morita, K. Suzuya, M.C. Weber and C.J. Benmore: Proc. Natl. Acad. U. S. A., **108** (2011) 14780, DOI: 10.1073/pnas.1104692108.
8) K. Shimoda, Y. Tobu, M. Hatakeyama, T. Nemoto and K. Saito: Am. Mineral., **92** (2007) 695, DOI: 10.2138/am.2007.2535.
9) M.C. Wilding, C.J. Benmore and J.K.R. Weber: J. Mater. Sci., **43** (2008) 4707, DOI: 10.1007/s10853-007-2356-5.
10) O.B. Fabrichnaya: CALPHAD, **24** (2001) 113-131, DOI: 10.1016/S0364-5916(00)00019-5.
11) J.W. Tomlinson, M.S.R. Heynes and J.O'M. Bockris: Trans. Faraday Soc., **54** (1958) 1822, DOI: 10.1039/TF9585401822.
12) T.B. King: J. Soc. Glass Technol., **35** (1951) 241.
13) H. Tokunaga, S. Ideguchi, F. Shimizu, N. Saito and K. Nakajima: J. Jpn. Inst. Metals, **71** (2007) 445 (in Japanese), DOI: 10.2320/jinstmet.71.445.
14) D. Springorum: Slag Atlas, 2nd. Ed., Verlag Stahleisen GmbH (1995).
15) E.A. Hoffmann: Berg-Hüttenmänn. Monatsh., **106** (1959) 397.
16) E.F. Riebling: Canad. J. Chem., **42** (1964) 2811.
17) J.O'M. Bockris, J.D. Mackenzie and J.A. Kitchener: Trans. Faraday Soc., **51** (1955) 1734, DOI: 10.1039/TF9555101734.
18) G. Urbain, Y. Bottinga and P. Richet: Geochim. Cosmochim. Acta, **46** (1982) 1061, DOI: 10.1016/0016-7037(82)90059-X.
19) T. Licko and V. Danek: Phys. Chem. Glasses, **27** (1986) 22.
20) L. Xie, A. Yoneda, D. Yamazaki, G. Manthilake, Y. Higo, Y. Tange, N. Guignot, A. King, M. Scheel and D. Andrault: Nat. commun., **11** (2020) 548, DOI: 10.1038/s41467-019-14071-8.
21) B.B. Karki, J. Zhang and L. Stixrude: Geophys. Res. Lett., **40** (2013) 94, DOI: 10.1029/2012GL054372.
22) W.-K. Rhim, S.-K. Chung, D. Barber, K.F. Man, G. Gutt, A.A. Rulison and R.E. Spjut: Rev. Sci. Instrum., **64** (1993) 2961. DOI: 10.1063/1.1144475.
23) S.K. Chung, D.B. Thiessen and W.-K. Rhim: Rev. Sci. Instrum., **67** (1996) 3175, DOI: 10.1063/1.1147584.
24) W.-K. Rhim, K. Ohsaka, P.-F. Paradis and R.E. Spjut: Rev. Sci. Instrum., **70** (1999) 2796, DOI: 10.1063/1.1149797.
25) H. Tamaru, C. Koyama, H. Saruwatari, Y. Nakamura, T. Ishikawa and T. Takada: Microgravity Sci. Technol., **30** (2018) 643, DOI: 10.1007/s12217-018-9631-8.
26) H. Oda, C. Koyama, M. Ohsio, H. Saruwatari and T. Ishikawa: Int. J. Microgravity Sci. Appl., **37** (2020) 370302, DOI: 10.15011/ijmsa.37.3.370302.
27) T. Ishikawa, C. Koyama, H. Oda, H. Saruwatari and P.-F. Paradis: Int. J. Microgravity Sci. Appl., **39** (2022) 390101, DOI: 10.15011/jasma.39.390101.

28) Lord Rayleigh: Proc. R. Soc. London, **14** (1882) 184.
29) H. Lamb: Hydrodynamics, 6th ed. (Cambridge University Press, Cambridge, 1932), p. 473.
30) N.M. Parikh: J. Am. Ceram. Soc., **41** (1958) 18, DOI: 10.1111/j.1151-2916.1958.tb13497.x.
31) W.D. Kingery: J. Am. Ceram. Soc., **42** (1959) 6, DOI: 10.1111/j.1151-2916.1959.tb09134.x.
32) S. Sukenaga and H. Shibata: Materia Japan, **58** (2019) 627, DOI: 10.2320/materia.58.627.
33) J. Paras, O. Takeda, M. Wu, and A. Allanore: Met. Mat. Trans., **53B** (2022) 2077, DOI: 10.1007/s11663-022-02508-3.
34) A. Masuno, C. Koyama, S. Kohara, S. Sasaki, S. Izumi, T. Matsuya, Y. Mikami, K. Yoshida, H. Kobayashi, Y. Watanabe, A. Mizuno, H. Oda, Y. Shuseki, M. Watanabe, J.T. Okada and T. Ishikawa: npj microgravity, **11** (2025) 58, DOI: 10.1038/s41526-025-00520-w.
35) S.K. Wilke, T. Ishikawa, C. Koyama, C.J. Benmore, A.L. Kastengren, A. Al-Rubkhi, J. Rafferty and R. Weber: J. Am Ceram. Soc., **109** (2026) e70573, DOI: 10.1111/jace.70573.
36) S.K. Wilke, A. Al-Rubkhi, V. Menon, J. Rafferty, C. Koyama, T. Ishikawa, H. Oda, R.W. Hyers, R.C. Bradshaw, A.L. Kastengren, S. Kohara, M. SanSoucie, B. Phillips and R. Weber: Appl. Phys. Lett,. **124** (2024) 264102, DOI: 10.1063/5.0198322.
37) J. Nawer, T. Ishikawa, H. Oda, H. Saruwatari, C. Koyama, X. Xiao, S. Schneider, M. Kolbe and D.M. Matson: npj microgravity**, 9** (2023) 38, DOI: 10.1038/s41526-023-00277-0.
38) T. Ishikawa, H. Oda, C. Koyama, R. Shimonishi, R. Ikeuchi, P.-F. Paradis, J.T. Okada, H. Fukuyama and H. Yamano: Int. J. Microgravity Sci. Appl., **42** (2025) 420202, DOI: 10.15011/jasma.42.420402.
39) T. Masaki, S. Murata, T. Takekawa, S. Shikichi, H. Kobatake, S. Shiratori, S. Ozawa, H. Oda, C. Koyama, R. Shimonishi, T. Ishikawa and K. Nagayama: Int. J. Microgravity Sci. Appl.**, 42** (2025) 420402, DOI: 10.15011/jasma.42.420402.
40) K. Mori, N. Minagawa, T. Ishikawa, C. Koyama, H. Oda and Y. Watanabe: Int J. Microgravity Sci. Appl., **43** (2026) 430101, DOI: 10.15011/jasma.43.430101.
41) Y. Kushiya, K. Kadoi, H. Ueno, Y. Mabuchi, C. Hanada, Y. Ueda, R. Saguchi, M. Yamada, H. Sato, Y. Watanabe, C. Koyama, H. Oda, T. Ishikawa, Y. Watanabe, and S. Suzuki: Int. J. Microgravity Sci. Appl., **43** (2026) 430202, DOI: 10.15011/jasma.43.430202.
42) Y. Seimiya, H. Kobatake, R. Sugahara, S. Kurosawa, K. Tono-oka, S. Shiratori, K. Sugioka, T. Ishikawa and S. Ozawa: ISIJ Int., **64** (2024) 2253, DOI: 10.2355/isijinternational.ISIJINT-2024-277.
43) Y. Seimiya, T. Suzuki, A. Mio and S. Ozawa: Int. J. Microgravity Sci. Appl.**, 42** (2025) 420301, DOI: 10.15011/jasma.42.420301.

Appendix-A

The effect of the frequency offset (defined as a difference of forced oscillation frequency and mode-2 oscillation frequency) on the surface tension and viscosity measurements was experimentally verified in the ISS-ELF using an Au sample whose mass was 59 mg. The sample was levitated, melted and kept at 1400 °C. The sample was oscillated with 11 different forced oscillation frequencies, ranging from 116 to 136 Hz with 2 Hz intervals.

Some of the obtained oscillation signals are shown in **Fig. A1**. Profile of the oscillation signal during free decay differed with different frequency offsets. **Figure A1(d)** shows the peak power of the oscillation calculated in the FFT analysis. From this figure, it is obvious that the mode-2 oscillation frequency of this sample was around 124 Hz.

The peak frequencies (f_2) from the FFT analysis and the calculated surface tensions are plotted as a function of forced oscillation frequency in **Fig.A2(a)**. The measured f_2 is almost constant (ranging from 124.5 to 125.1 Hz), thus surface tension values are independent from the frequency offset.

The measured decay constant (t) and the viscosity are plotted in **Fig. A2(b)**. The *t* is strongly affected by the frequency offset as shown in **Fig.A2(b)**. The larger the frequency offset is, the smaller is t and the larger is the viscosity.

The measured viscosities with forced oscillation frequencies 124 and 126 Hz (whose frequency offset is within 2 Hz) are around 3.8 mPa·s. These viscosity values agree well with the literature data (3.56 mPa·s by Ofte[1)]), while the obtained viscosity values with bigger frequency offset (more than 2 Hz) are at least 25% larger than the literature ones.

The same results have also been confirmed in the experiments with Pt and Nb_2O_5 samples. Moreover, the sample deformation of these samples was observed through the images recorded by a high speed camera[2)].

It is important to minimize the frequency offset as much as possible to obtain precise viscosity values.

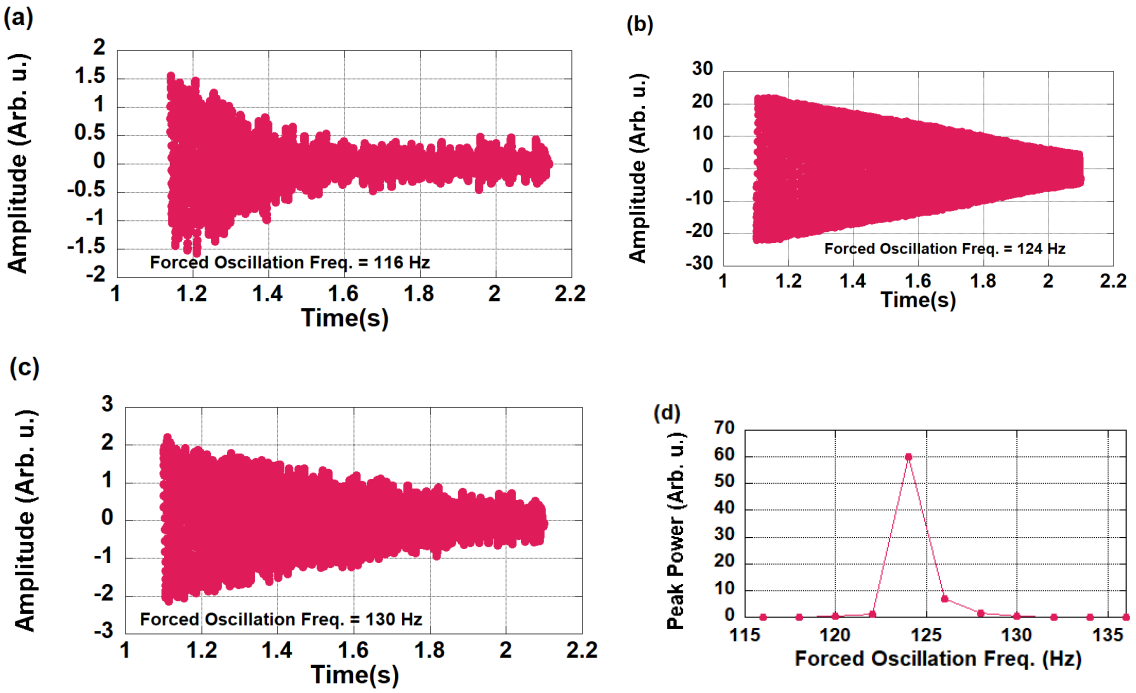


Figure A1. Filtered oscillation signal of Au with 3 different forced oscillation frequencies (a)116 Hz, (b) 124 Hz, and (c) 130 Hz. Raw signals were filtered with a 100-200 band pass filter. Peak power obtained from FFT analysis is shown in (d).

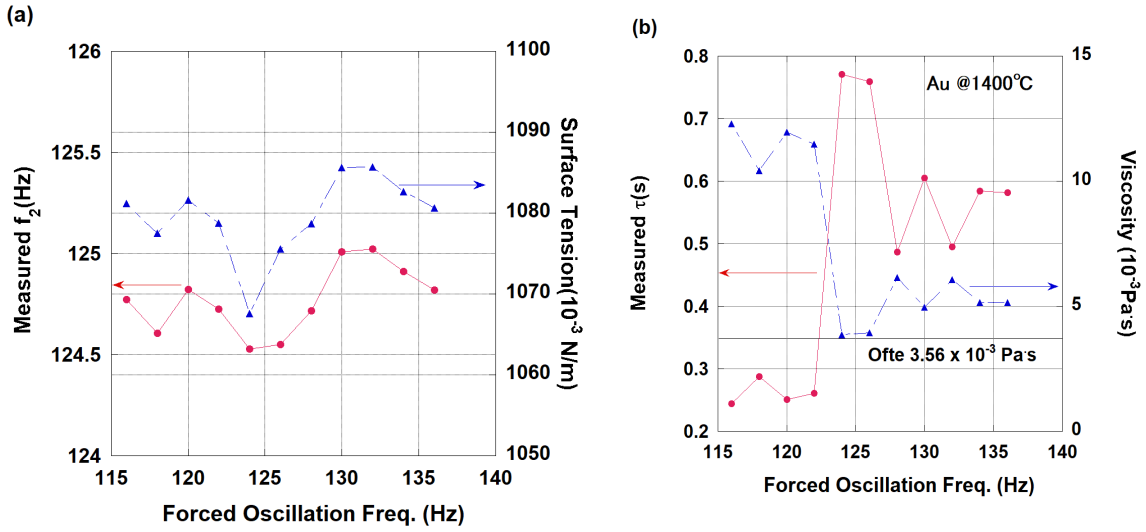


Figure A2. (a) Measured f_2 and calculated surface tension vs forced oscillation frequency. (b) measured τ and calculated viscosity vs forced oscillation frequency.

1) D. Ofte: J. of Nuclear Materials, **22** (1967) 28, DOI: 10.1016/0022-3115(67)90105-5.
2) T. Corbin, J. Liversay, T. Ishikawa, C. Koyama, M. Sansoucie, B. Phillips and R. Narayanan: npj microgravity, **12** (2026) 38, DOI: 10.1038/s41526-026-00585-1.

Appendix-B

Figure B1 shows a typical oscillation signal and FFT results obtained for an Au sample.

The peak indicated in a thin arrow corresponds to the lateral sample movement due to the input forced oscillation (61 Hz), and the largest peak in a bold arrow (122 Hz) is derived from the sample surface

deformation. This second peak indicates that the sample is molten and its viscosity is low enough to show the observable deformation.

A typical oscillation signal and the FFT result obtained for 50MgO are shown in **Fig. B2**.

Focusing on the FFT result of 50MgO, no second peak can be observed, which indicates that the sample viscosity is very high and observable deformation cannot be made by current ISS-ELF system.

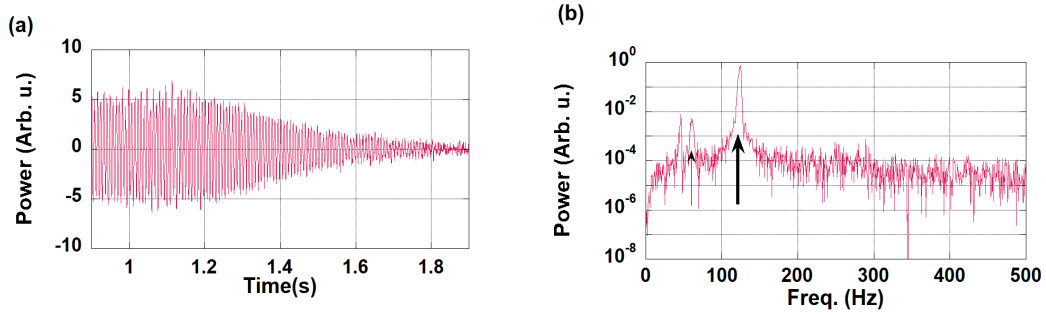


Figure B1. Oscillation signal of Au (a) and its FFT result (b). Raw signal was filtered with a 40-500 Hz band pass filter.

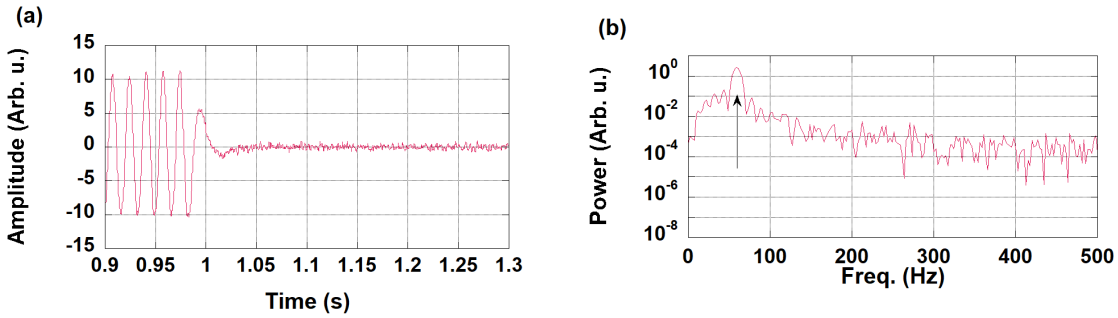


Figure B2. Oscillation signal of 50MgO (a) and its FFT result (b). Raw signal was filtered with a 40-500 Hz band pass filter.

© 2026 by the authors. Submitted for possible open access publication under the terms and conditions of the Creative Commons Attribution (CC BY) license (http://creativecommons.org/licenses/by/4.0/).